Control Scheme for Wide-Bandgap Motor Inverters with an Observer-Based Active Damped Sine Wave Filter

F. Maislinger and H. Ertl, TU-Wien, Institute of Energy Systems and Electrical Drives,
A-1040 Vienna, Austria, franz.maislinger@tuwien.ac.at
G. Stojcic, C. Lagler and F. Holzner, B&R Industrial Automation GmbH, A-5142 Eggelsberg, Austria

Abstract

This paper presents an effective method for the active damping of a two-stage sine wave LC output filter for wide-bandgap motor inverters avoiding any sensing of filter voltages/currents. The method is based on a linear observer model, which is used for estimating the filter capacitor currents required for implementing the active damping. The motor currents are controlled using a conventional PI-type controller with additional feedback based on the estimated filter capacitor currents. Using the proposed method, the inverter's standard output current sensing can be used also in case of active filter damping avoiding any additional measurement channels and dissipative losses, which appear in case of passive filter damping. The paper reports the operating principle and analyzes the stability region and robustness of the total system by simulations. Finally, the proposed scheme is tested by implementation of a laboratory inverter prototype based on GaN-MOSFETs at a switching frequency of 100 kHz.

1. Introduction

Today, silicon (Si) based insulated gate bipolar transistors (Si-IGBTs) operating in pulse width modulation (PWM) mode at switching frequencies up to 20 kHz are commonly used for the implementation of motor inverters in the kW domain. During the past few years, however, wide-bandgap switching devices like GaN- and SiC MOSFETs have considerably emerged, also in inverter applications based on 600 V GaN devices. The wide bandgap, associated with the high critical electrical field of GaN and the high electron mobility principle (HEMT) has led to very impressive new power transistors [1]. The low semiconductor capacitances of GaN as well as advances in packaging technologies facilitate very high switching speed resulting in substantially lower switching losses in comparison to silicon (Si) based IGBTs. Low switching- and also low on-state losses of GaN MOSFETs now enable motor inverters operating at high switching frequencies with high efficiency rates [2].

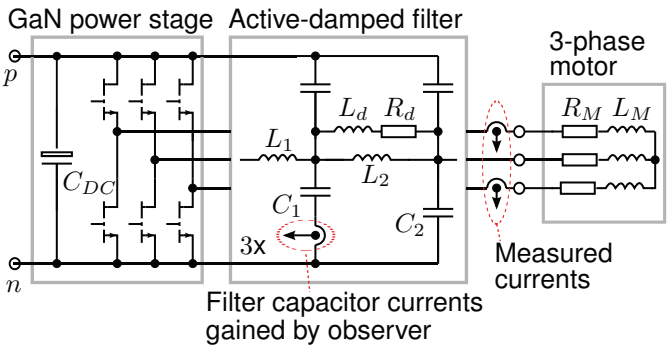

Fig. 1: Basic concept of the proposed motor inverter with GaN power stage and actively damped symmetrical two-stage filter for a 3-phase motor load.

The very fast switching in the nanosecond range at 400 V DC-link voltage however creates some crucial issues for motor applications using standard 3-phase / two level inverters. Transient overvoltages at the motor terminals caused by the high du/dt rates of more than 50 kV/µs may impair winding isolation and reduce the lifetime of motors [3]. Furthermore, additional load currents due to cable capacitances and motor voltage ringing limit the maximum cable length and increase switching losses of the inverter.

The high switching speed of GaN MOSFETs on the other hand, facilitates switching frequencies of 100 kHz and above, which make an output filter possible that can be directly implemented into the inverter. This LC filter substantially suppresses most of the switching frequency harmonics to obtain sinusoidal-like inverter output voltages. Consequently, as reported in [2], by avoiding high frequency motor and cable losses the total system efficiency is expected to be increased. Furthermore, it seems to be possible to avoid shielded motor cables resulting in a

ISBN 978-3-8007-4646-0

cost and application benefit. A schematic outline of the proposed inverter system is depicted in Fig. 1. Here, to achieve a sufficient switching noise suppression but also rather high control bandwidth as being necessary for servo drives, at least a two-stage LC sine wave filter is required [4]. The filter is designed such that the noise level at the inverter‘s output comply with common industrial standards. In this paper the standard IEC/EN 55011 class-A is considered.

Nevertheless, the LC filter resonances have to be damped for actual implementations and for proper control loop design. For this, frequently dissipative components are used, leading however to additional losses decreasing the system efficiency. As an improvement in [5], e.g., the filter resonances are damped by a hybrid structure consisting of a single-stage LC filter with a resonance tank in parallel to the LC stage capacitor in connection with a digital notch filter. The resonance tank (LCR series circuit) is tuned to the switching frequency, the damping resistor acts for the tank as well as for the main LC stage. Nevertheless, the damping resistor leads to additional dissipative losses and so a trade-off has to be taken between the occurring output voltage overshoot and the filter losses.

To effectively avoid filter damping losses an active damping concept by capacitor current feedback is proposed in [6]. The sensed filter capacitor current is multiplied by a coefficient k_d and fed back to the PWM stage with negative sign. This emulates a kind of ohmic, but not dissipative, damping resistor resulting into a well damped system, if k_d is properly matched to the filter parameters L and C. However, this approach requires knowledge of the inner filter state variables, consequently leading to additional sensing channels, which are often not available or only by additional costs.

In this paper, to obtain high inverter efficiencies but avoiding the mentioned additional sensing channels, the proposed concept in [6] is extended by an observer model, which estimates the required capacitor filter currents for active damping. The following section shows the observer-based active damping concept as well as a corresponding design for a conventional PI controller. Furthermore, the influence of parameter variations on the system stability is also discussed.

2. Control Scheme

For the analysis of the motor current control applying the proposed observer-based active damping, a single-phase equivalent circuit of the inverter and the two-stage LC output filter as shown in Fig. 2 is used. Here, it is assumed that the GaN power stage block acts as a transfer function of gain $\nu = 1$. The motor load is specified by a $L_M R_M$ element in combination with a voltage source u_{emf} representing the induced motor voltage.

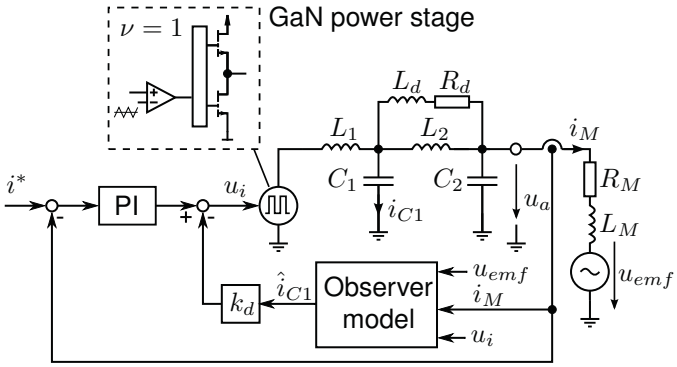

Fig. 2: Proposed closed-loop control using a PI-type controller for motor current control employing additional feedback of the observed filter capacitor current $\hat{i}_{C1}$.

The LC filter resonance frequencies have to be well between the maximum electrical motor operation frequency f_{el} and the inverter switching frequency f_s, i.e. $f_{el} << f_{res} << f_s$. To achieve a sufficient attenuation of the switching noise but also a rather high current control bandwidth, the corresponding filter parameters are specified in [6] and listed in Table 1. In contrast to passive damping schemes, which reduce the system efficiency due to additional dissipative losses, the resonance of the first filter-stage now is attenuated by a feedback of the filter capacitor current i_{C1}. Using an adequate feedback parameter k_d, which can be approximated by

$$k_d = 2\xi\sqrt{\frac{(L_1 + L_M)\, L_1}{C_1 L_M}},\ \xi = 0.9, \qquad (1)$$

the feedback acts like an ohmic resistor resulting in a well damped dynamic of the controlled plant. However, instead of an additional current measurement for i_{C1}, the filter capacitor current is estimated

by a linear observer model which maps the differential equations of the dynamic system. It has to be noted, that the second LC filter-stage still uses a small dissipative damper $R_d L_d$ (parallel branch to L_2). This is because the resonance frequency defined by the parameters $L_2 C_2$ is about 3-times higher as for the first stage and the bandwidth limit of the digital PWM and control of the bridge leg is not sufficient for a very effective damping of $L_2 C_2$. The losses in R_d, however, are almost negligible.

Tab. 1: Parameter settings of implemented system.

Part	Parameter	value	unit
Inverter	U_{DC}	400	V
	C_{DC}	120	µF
	f_s	100	kHz
Sine-Filter	L_1	200	µH
	R_1	110	mΩ
	C_1	2.5	µF
	L_2	25	µH
	R_2	30	mΩ
	C_2	2.5	µF
	L_d	33	µH
	R_d	5.6	Ω
Motor	L_M	4.4	mH
	R_M	0.48	Ω
	I_M	6	A
	U_M	400	V
	$2p$	10	
	n_M	3000	min^{-1}
Controller	T_s	10	µs
	T_I	0.476	ms
	V_I	$5.04e4$	V A^{-1}
	k_d	12.0	V A^{-1}
Observer	$\mathbf{k}_{OB}[1]$	0.5	
	$\mathbf{k}_{OB}[2\text{-}5]$	0	
	$\mathbf{k}_{OB}[6]$	-0.2	

2.1. Observer Model

In the following, a linear observer model corresponding to the dynamic plant of the inverter is implemented. Fig. 2 shows the dynamic plant of a single-phase system with two input quantities: The voltage u_i describes the input value of the system, whereas the internal induced voltage u_{emf} acts as an external disturbance to the system and does not affect its stability. Nevertheless, its knowledge is necessary for the observer model. Both variables can be combined to the vector $\mathbf{u} = [u_i, u_{emf}]^T$. For controlling the motor current, i_M is measured and therefore is

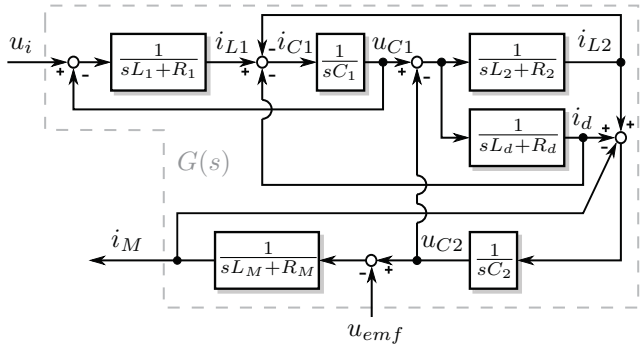

Fig. 3: Plant dynamic model including two-stage filter and a $R_M L_M$ path as motor load. The parameters R_1 and R_2 take into account the ohmic copper losses of the two inductors.

known for the observer design. From the resulting system differential equations

$$\frac{\mathrm{d}}{\mathrm{d}t} i_{L1}(t) = \frac{-R_1 i_{L1} - u_{C1} + u_i}{L_1}, \tag{2a}$$

$$\frac{\mathrm{d}}{\mathrm{d}t} u_{C1}(t) = \frac{i_{L1} - i_{L2} - i_d}{C_1}, \tag{2b}$$

$$\frac{\mathrm{d}}{\mathrm{d}t} i_{L2}(t) = \frac{-R_2 i_{L2} + u_{C1} - u_{C2}}{L_2}, \tag{2c}$$

$$\frac{\mathrm{d}}{\mathrm{d}t} u_{C2}(t) = \frac{i_{L2} + i_d - i_M}{C_2}, \tag{2d}$$

$$\frac{\mathrm{d}}{\mathrm{d}t} i_d(t) = \frac{-R_d i_d + u_{C1} - u_{C2}}{L_d}, \tag{2e}$$

and

$$\frac{\mathrm{d}}{\mathrm{d}t} i_M(t) = \frac{-R_M i_M + u_{C2} - u_{emf}}{L_M}, \tag{2f}$$

a state space model in the continuous time domain can be obtained in the form

$$\dot{\mathbf{x}} = \mathbf{A}\mathbf{x} + \mathbf{B}\mathbf{u}, \tag{3a}$$

$$y = \mathbf{c}^T \mathbf{x}, \tag{3b}$$

with $\mathbf{x} = [i_{L1}, u_{C1}, i_{L2}, u_{C2}, i_d, i_M]^T$ (corresponding to the six state variables), the output vector $\mathbf{c} = [0, 0, 0, 0, 0, 1]^T$, as well as the matrices

$$\mathbf{A} = \begin{bmatrix} -\frac{R_1}{L_1} & -\frac{1}{L_1} & 0 & 0 & 0 & 0 \\ \frac{1}{C_1} & 0 & -\frac{1}{C_1} & 0 & -\frac{1}{C_1} & 0 \\ 0 & \frac{1}{L_2} & -\frac{R_2}{L_2} & -\frac{1}{L_2} & 0 & 0 \\ 0 & 0 & \frac{1}{C_2} & 0 & \frac{1}{C_2} & -\frac{1}{C_2} \\ 0 & \frac{1}{L_d} & 0 & -\frac{1}{L_d} & -\frac{R_d}{L_d} & 0 \\ 0 & 0 & 0 & \frac{1}{L_M} & 0 & -\frac{R_M}{L_M} \end{bmatrix} \tag{4a}$$

ISBN 978-3-8007-4646-0

and

$$\mathbf{B} = \begin{bmatrix}\mathbf{b}_1 & \mathbf{b}_2\end{bmatrix} = \begin{bmatrix} \frac{1}{L_1} & 0 & 0 & 0 & 0 & 0 \\ 0 & 0 & 0 & 0 & 0 & -\frac{1}{L_M} \end{bmatrix}^T . \quad (4b)$$

By using the Popov-Belevitch-Hautus (PBH) eigenvector test [7], it can be seen that the obtained system is completely observable, if the condition

$$L_2 R_d \neq L_d R_2$$

is valid. It has to be noted, that a numerical calculation of the complete observability in a Matlab calculation has failed cause of numerical inaccuracies induced by the chosen parameters listed in Table 1. However, if the condition is not met, the eigenvalues of the occurring null dynamic of the investigated system must be considered, which corresponds for linear systems to the zeros of $G(s) = \mathbf{c}^T(s\mathbf{E} - \mathbf{A})^{-1}\mathbf{b}_1$. Here, the zero of $G(s)$ has a negative eigenvalue, which implicates an exponentially stable null dynamic. Thus, in both cases an observer for estimating the filter capacitor current i_{C1} can be modelled. For a digital implementation, the observer can be written in a discrete form as

$$\hat{\mathbf{x}}_{k+1} = \mathbf{\Phi}\hat{\mathbf{x}}_k + \mathbf{\Gamma}\mathbf{u}_k + \mathbf{k}_{OB}\left(\hat{y}_{1,k} - y_{1,k}\right), \quad (5a)$$

$$\hat{\mathbf{y}}_k = \begin{bmatrix}\hat{y}_{1,k} \\ \hat{y}_{2,k}\end{bmatrix} = \begin{bmatrix} & & \mathbf{c}^T & & & \\ 1 & 0 & -1 & 0 & -1 & 0 \end{bmatrix}\hat{\mathbf{x}}_k, \quad (5b)$$

where $\hat{y}_{2,k}$ conforms to $\hat{i}_{C1}$ and k to a discrete time step of length $T_s = 1/f_s$. The discrete matrices

$$\mathbf{\Phi} = \exp(\mathbf{A}T_s),\ \mathbf{\Gamma} = \int_0^{T_s} \exp(\mathbf{A}\tau)d\tau\mathbf{B}$$

can be obtained by the zero-order hold discretization of $\mathbf{A}$ and $\mathbf{B}$ with a sampling period T_s. In order to obtain a stable error system

$$\mathbf{e}_{k+1} = \hat{\mathbf{x}}_{k+1} - \mathbf{x}_{k+1} = \left(\mathbf{\Phi} + \mathbf{k}_{OB}\mathbf{c}^T\right)\mathbf{e}_k, \quad (6)$$

with $\mathbf{e}_k = \hat{\mathbf{x}}_k - \mathbf{x}_k$, the values of $\mathbf{k}_{OB}$ are chosen in a form that the error dynamic matrix $(\mathbf{\Phi} + \mathbf{k}_{OB}\mathbf{c}^T)$ becomes exponentially stable, for which Ackermann's formula can be used [8]. Inserting (5b) and (6) in (5a) leads to the resulting observer model

$$\hat{\mathbf{x}}_{k+1} = \mathbf{A}_{OB}\hat{\mathbf{x}}_k + \mathbf{B}_{OB}\begin{bmatrix}\mathbf{u}_k \\ y_{1,k}\end{bmatrix}, \quad (7a)$$

$$\hat{\mathbf{y}}_k = \mathbf{C}_{OB}\hat{\mathbf{x}}_k, \quad (7b)$$

with $\mathbf{A}_{OB} = \mathbf{\Phi} + \mathbf{k}_{OB}\mathbf{c}^T$, $\mathbf{B}_{OB} = [\mathbf{\Gamma}, -\mathbf{k}_{OB}]$ and $\mathbf{C}_{OB}$ appropriate to (5b). The filter current $\hat{i}_{C1}$ obtained from the observer now acts as an approximation of the actual current in the capacitor C_1 and in case of sufficient small parameter variations, it can be used for the proposed active damping concept.

2.2. Current Control

For controlling the motor currents, a closed-loop control concept using a conventional PI-type controller with a transfer function

$$R(z) = V_I\left(T_I + \frac{T_s}{2}\right) + \frac{T_s V_I}{z-1} \quad (8)$$

in the complex z-domain, with the controller parameters V_I and T_I, employing additional feedback of the observed capacitor currents is proposed. For calculating the controller parameters, it is assumed that the filter capacitor current required for the active damping concept is available as a measured value. Therefore, the transfer function $G(s)$ is divided into two parts, which can be modelled by

$$G_{z1}(z) = \frac{z-1}{z}\mathbf{Z}\left(\frac{1}{s}\frac{i_{C1}(s)}{u_i(s)}\right), \quad (9a)$$

$$G_{z2}(z) = \frac{z-1}{z}\mathbf{Z}\left(\frac{1}{s}\frac{i_M(s)}{i_{C1}(s)}\right), \quad (9b)$$

for a digital implementation in the z-domain (Fig. 4). Hence, in discrete time domain, the transfer function of the actively damped system leads to

$$G(z) = \frac{z^{-1}U_{DC}G_{z1}(z)}{1 + k_d z^{-1}U_{DC}G_{z1}(z)}G_{z2}(z), \quad (10)$$

where the inverter is modelled as a linear U_{DC} gain with a sample delay z^{-1} to account for PWM transport delay [9]. The active damping parameter k_d has to be chosen that a well damped behaviour occurs. As mentioned above, in continuous time

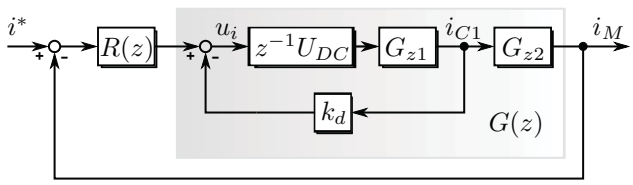

Fig. 4: Proposed closed-loop control concept in z-domain without observer.

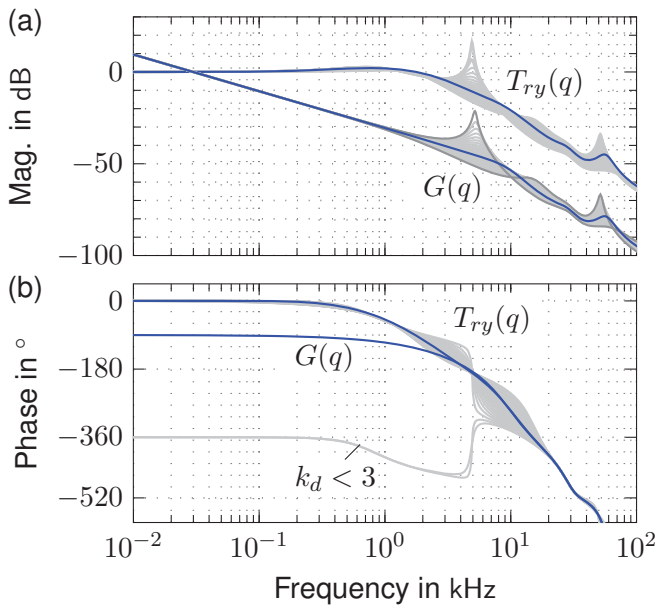

Fig. 5: Bode plot of dynamic plant and of the closed-loop transfer function for different active damping parameters $k_d = 1 \ldots 30$ (gray) as well as for $k_d = 12\,\mathrm{V\,A^{-1}}$ (blue), (a) magnitude, (b) phase.

domain, k_d can be calculated by (1), however, in a digital implementation, a phase shift introduced by the sampling process and the processing delay can destabilize a design that is stable in continuous time domain [10]. The influence of different active damping parameters k_d on the transfer function of the discrete dynamic plant is illustrated in Fig. 5. For this, by applying a bilinear Tustin transformation with pre-warping [11], $G(z)$ is rewritten as $G(q)$ for a sampling time of $T_s = 10\,\mu\mathrm{s}$, where the expression

$$z = \frac{1 + qT_s/2}{1 - qT_s/2} \tag{11}$$

maps the unit circle of the complex z-plane to the complex axis in the q-plane, with the new frequency parameter $q = 2\omega/T_s$. As depicted in the blue curves of Fig. 5, a well damped system behaviour can be obtained with an active damping parameter $k_d = 12\,\mathrm{V\,A^{-1}}$. Now, it is possible to calculate the closed-loop transfer function of the discrete system as

$$T_{ry}(q) = \frac{R(q)G(q)}{1 + R(q)G(q)}, \tag{12}$$

using a PI controller $R(q) = V_I\,(1 + qT_I)\,/q$. As can be seen in Fig. 5, the transfer function for a well damped system only has one intersection with the $0\,\mathrm{dB}$-line. Thus a frequency response method can

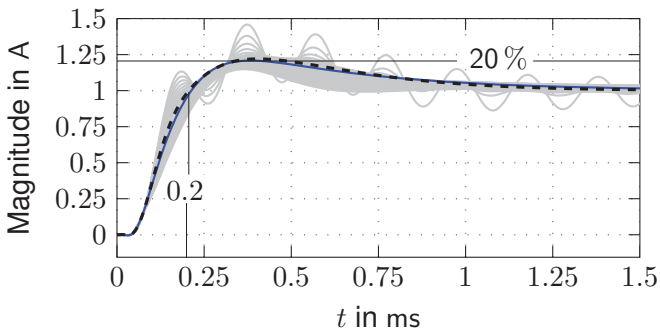

Fig. 6: Current step-responses of the closed-loop control for different active damping parameters (gray), for $k_d = 12\,\mathrm{V\,A^{-1}}$ (blue) as well as of the implemented model in *Matlab/Simulink* (dashed) for nominal filter parameters.

be used to determine the controller parameters V_I and T_I. These values depend on the rise time, the desired overshoot and the motor inductance. Here, the chosen characteristics of the step response with $20\,\%$ overshoot and a rise time of $0.2\,\mathrm{ms}$ lead to the controller parameters $V_I = 50.4\,\mathrm{kV\,A^{-1}}$ and $T_I = 0.48\,\mathrm{ms}$. Fig. 5 depicts the obtained closed-loop transfer function for different active damping parameters k_d. As can be seen, for $k_d < 3\,\mathrm{V\,A^{-1}}$ unstable closed-loop functions occur. The resulting motor current step responses for the proposed control scheme are illustrated in Fig. 6. Here, only active damping parameter values corresponding to a stable system behaviour are considered. Furthermore, the proposed control concept by using the observer for estimation of the filter capacitor current is implemented in *Matlab/Simulink* and tested with the obtained controller and active damping parameters. A single-phase equivalent circuit of the model is shown in Fig. 7, where a zero-order-hold part is used to switch the discrete system input u_i on the continuous dynamic plant $G(s)$. For nominal filter- and motor- values, the obtained step response corresponds to the desired behaviour (see Fig. 6 - dashed curve).

2.3. Influence of Parametric Variation

This section discusses the effects of parametric variations on the previously designed closed-loop system with observer-based active damped filter. Component tolerances of the used filter capacitors C_1 and C_2 as well as saturation effects of the inductors L_1, L_2 and L_M can affect the system stability.

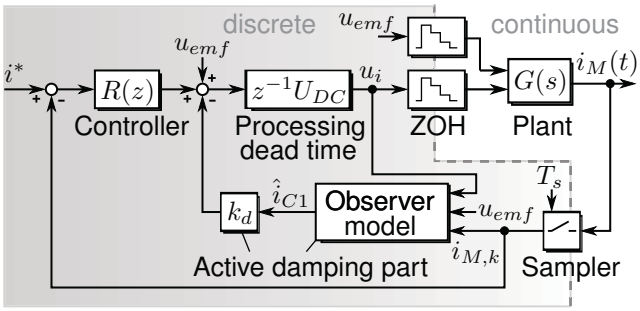

Fig. 7: Proposed closed-loop control concept of a single phase model implemented in *Matlab/Simulink*.

Due to the passive damping of the second filter-stage, the varying parameters are constrained to L_1, C_1 and L_M. To perform the analysis, the active damping- as well as the controller parameters are calculated for the nominal values of the two-stage filter as listed in Table 1. For the simulation, the *Matlab/Simulink* model illustrated in Fig. 7 is used. Then, each of the filter parameters is varied in a range of $-50\,\%$ to $+50\,\%$, for motor inductances $0.4L_{M,nom} \leq L_M \leq 1.4L_{M,nom}$. Fig. 8 depicts the lower stability limit for different values of L_M. As indicated, for the nominal motor inductance, the system has a stable behaviour for a parametric variation of $-20\,\%$ in L_1 and C_1. At $60\,\%$ reduced motor inductance, the allowed deviation of the filter parameters however is only $-10\,\%$. Furthermore, for $L_M = 0.6L_{M,nom}$ and $L_1 = 1.5L_{1,nom}$, the condition $L_M > 10L_1$ is no longer satisfied, so the mismatch of active damping increases the overshoot and the whole system becomes unstable. By increasing the motor inductance, the robustness of the system can be increased slightly, however, larger values of L_M reduce the closed-loop system dynamic.

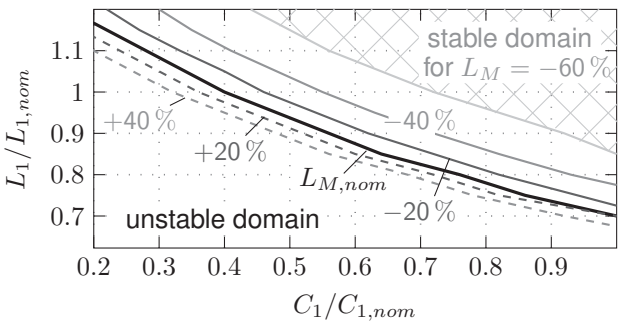

Fig. 8: Lower stability limit for different values of motor inductance L_M. The region above the different curves indicates the stable domain.

3. Experimental Results

In order to verify the proposed control and observer-based active damping concept, a 2 kW/400 V laboratory prototype has been implemented. Filter- and motor parameters as well as design specifications are given in Table 1.

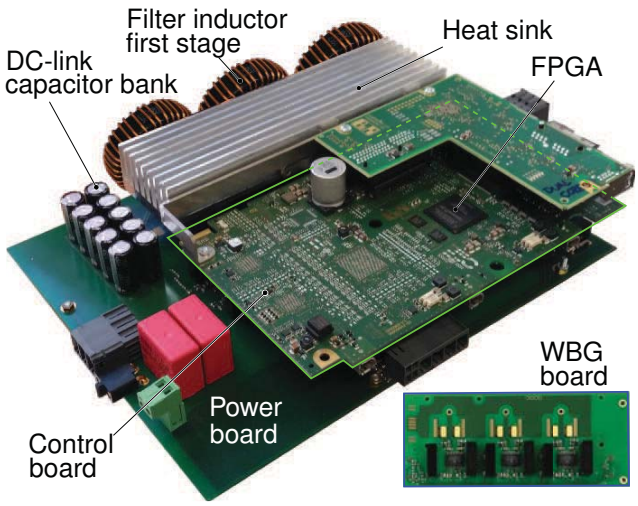

Fig. 9: Laboratory prototype consisting of power-, WBG- and control-board. Power-board dimensions: 200 mm x 250 mm.

As illustrated in Fig. 9, the prototype mainly consists of three PCB boards: A GaN transistor carrier-(WBG), a basic power- and a control-board. A separate WBG-board placed under the heat sink, is used to test different wide bandgap transistors and Gate drivers. Here, the half-bridges (formed by 2 GaN-HEMTs GS66508T) are controlled by Si82394 isolator/drivers, which feature fully isolation, 4 A output current capability and include also programmable interlock delay, adjusted to 150 ns. It has to be remarked, that high switching frequencies reduce the inverter/filter volume on the one hand, but on the other hand, the switching losses are increased. Accordingly the cooling system volume increases, compensating the filter volume savings. Beside this fact, the efficiency is also reduced. Consequently, as a compromise for high inverter efficiency and low volume, the switching frequency of the GaN power stage is set to 100 kHz.

A standard motion control-board is taken from B&R Industrial Automation GmbH. It includes an embedded system, where the discussed current control- as well as the observer-based active damping con-

ISBN 978-3-8007-4646-0

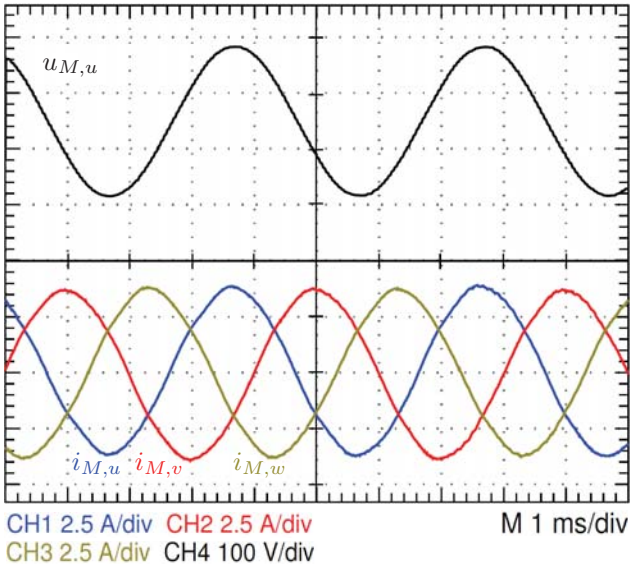

Fig. 10: Measured motor currents $i_{M,u}$, $i_{M,v}$, $i_{M,w}$ and motor voltage $u_{M,u}$ for an external load of 2.5 N m at a motor operating frequency of $f_{el} = 250$ Hz .

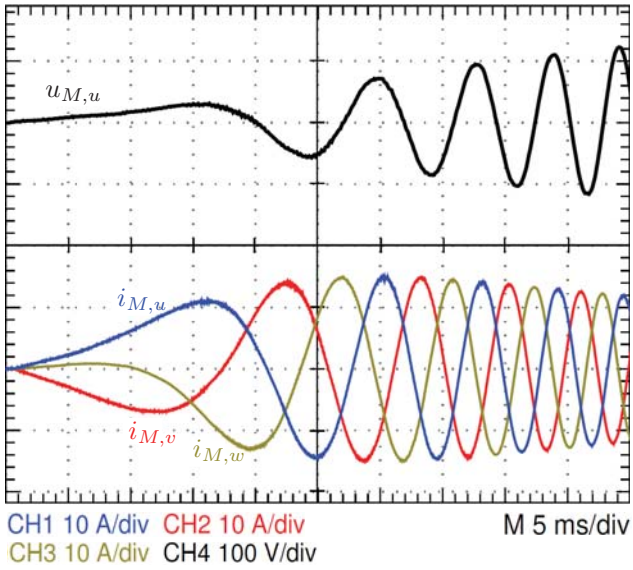

Fig. 11: Measured motor currents $i_{M,u}$, $i_{M,v}$, $i_{M,w}$ and motor voltage $u_{M,u}$ for a speed increase from standstill to 3000 min^{-1} within 60 ms.

cept is implemented for each motor phase. A controller sampling time of $T_s = 10$ µs is used in single-edge sampling mode, PWM transport delay and current oversampling lead to a processing dead time of 10 µs. The approach of the proposed linear observer model is necessary to enable a fast and reliable calculation of the required state variables within one sampling period. It shall be noted, that a measurement of the filter capacitor current would add an additional sampling delay impairing dynamic behaviour and stability.

The two-stage filter, measurement circuits for currents and temperature, as well as the DC-link electrolytic capacitor bank are all placed on the main power-board. To reduce noise impacts, the required motor phase current measurements are realized by shunts in combination with a ACPL-798J second order sigma delta modulator, which oversamples the analog input signal into a high-speed data stream. As shown in Sec. 2.3, for the observer-based active damping scheme chokes with a sufficient linear behaviour with respect to the current as well as with a relatively high saturation current limit to meet the demands for servo motor applications are necessary. Hence, toroidal powder cores (L_1: Kool-Mμ-max, $\mu_r = 26$, ∅57.1 mm, 57 turns, L_2: Sendust, $\mu_r = 60$, ∅20.3 mm, 20 turns) are used for the inductors of the filter-stages. The coils are formed as single layer windings to minimize proximity effects, hence, standard copper wire is sufficient. To obtain a rather small filter volume, ceramic capacitors are used for the implemented two-stage filter, which easily can handle the switching frequency current ripple. However, the capacitance of most ceramic capacitors in this voltage domain shows a very pronounced nonlinear behaviour depending on the DC-bias voltage and this may influence the controllability of the inverter system. Fortunately, adequate C0G dielectric capacitors are recently available (Kemet KC-link, 220 nF, 500 V) showing a capacitance being almost independent of DC-bias voltage and therefore are used for the first filter-stage. For the second filter-stage, standard ceramic capacitors (Arcshield X7R, 500 V) are used for saving cost. It has been observed that their voltage dependency does not have severe impact on the output voltage quality and system stability.

In Fig. 10, the motor phase currents as well as the motor voltage $u_{M,u}$ in a stationary operating point, for an electrical frequency of 250 Hz and a mechanical load of 2.5 N m are shown. Due to the two-stage filter, both, the motor- currents as well as the motor/cable voltage show the expected sinusoidal shape with a rather small ripple. In Fig. 11, the occurring motor- currents and voltage for a speed increase from standstill to 3000 min^{-1} within a time

range of 60 ms are depicted. Here, small current and voltage distortions can be observed, induced by the high currents to bypass the starting torque of the permanent magnet synchronous machine (PMSM). In particular, for high currents the nonlinearity of the motor inductance as well as of the filter inductor result in a mismatch of the observer-based active damping scheme.

In order to demonstrate the stable behaviour of the proposed method, the system is further tested by a step change in load torque. For this purpose, the PMSM fed by the laboratory prototype is mechanically coupled to a second PMSM, whose phases are terminated by a 3-phase power resistor as illustrated in Fig. 12. In Fig. 13, the measured motor- as well as the observed filter capacitor current of one phase are illustrated for a step change in load of half nominal torque. As can be seen, the controlled motor current shows the desired sinusoidal shape and after a time of 30 ms the resulting drop of the rotational speed n is fully compensated.

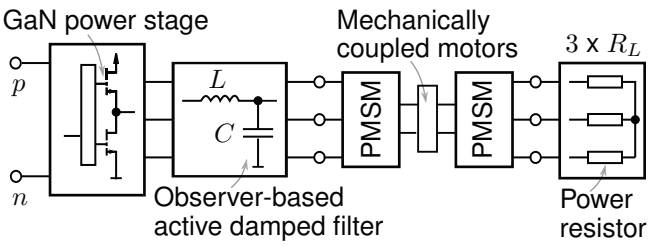

Fig. 12: Coupled motors for testing step changes in load.

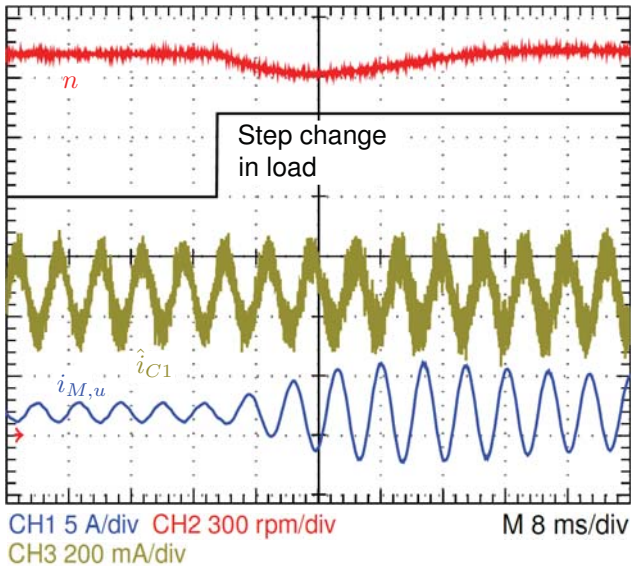

Fig. 13: Measured motor current $i_{M,u}$, and observed filter current $\hat{i}_{C1,u}$ for a step change in load of half nominal torque at a rotational speed of 1800 min^{-1}.

4. Conclusion

In this work, a control scheme for a 3-phase wide-bandgap inverter, operating at 400 V DC-link voltage at a PWM frequency of 100 kHz with an observer-based actively damped sine wave output filter is analyzed. In order to obtain high system efficiencies, the resonance of the first filter-stage is damped actively by feedback of the filter capacitor current avoiding additional losses caused by dissipative damping. Instead of additional current sensing channels, a linear observer model is proposed and designed for estimating the capacitor currents needed for active damping. The paper describes the applied closed-loop control scheme for a purely digital implementation, using a conventional PI-type controller. Furthermore, an analysis of the influence on filter parameter variations, which show the theoretical limits for a stable closed-loop controlled system, is performed. An implemented laboratory prototype feeding a mechanically coupled 3-phase PMSM is used for testing the proposed control concept. The measured motor- currents and voltages show a stable behaviour for step changes in load as well as the expected almost noise-free sinusoidal shape.

5. References

[1] A. Lidow, J. Strydom, M. de Rooij, and David Reusch. *GaN Transistors for Efficient Power Conversion*. John Wiley & sons, El Segundo, California, 2nd edition, 2015.

[2] K. Shirabe and M.M. Swamy. Advantages of high frequency PWM in AC motor drive applications. *Energy Conversion Congress and Exposition (ECCE)*, September 15-20 2012.

[3] P. Nussbaumer, C. Zoeller, T.M. Wolbank, and M.A. Vogelsberger. Transient distribution of voltages in induction machine stator windings resulting from switching of power electronics. *Industrial Electronics Society, IECON 2013 -*

39th Annual Conference of the IEEE, pages 3189–3194, 2013.

[4] P. Cortes, D.O. Boillat, H. Ertl, and J.W.Kolar. Comparative evaluation of multi-loop control schemes for a high bandwidth AC power source with a two-stage LC output filter. *Proceedings of the International Conference on Renewable Energy Research and Applications (ICRERA 2012)*, November 11-14 2012.

[5] F. Stubenrauch, N. Seliger, and D. Schitt-Landsiedel. Design and performance of a 200kHz GaN motor inverter with sine wave filter. *International Exhibition and Conference for Power Electronics, Intelligent Motion, Renewable Energy and Energy Management, PCIM Europe 2017*, May 16 - 18 2017.

[6] F. Maislinger, H. Ertl, G. Stojcic, C. Lagler, and F. Holzner. Design of a 100kHz wide bandgap-inverter for motor applications with active damped sine wave filter. *International Conference on Power Electronics, Machines and Drives (PEMD 2018)*, April 17-19 2018.

[7] B. K. Ghosh and J. Rosenthal. A generalized Popov-Belevitch-Hautus test of observability. *IEEE Transactions on Automatic Control*, 40, January 1995.

[8] J. Ackermann. Parameter space design of robust control systems. *IEEE Transactions on Automatic Control*, 25:1058–1072, December 1980.

[9] S.G. Parker, B.P. McGrath, and D.G. Holmes. Regions of active damping control for LCL filters. *IEEE TRANSACTIONS ON INDUSTRY APPLICATIONS, VOL. 50*, pages 424–432, January 2014.

[10] J. Dannehl, F. Fuchs, S. Hansen, and P. Thorgersen. Investigation of active damping approaches for PI-based current control of grid-connected pulse width modulation converters with LCL filters. *IEEE Trans. Ind. Appl.*, 46:1509–1517, August 2010.

[11] K.J. Astrom and B. Wittenmark. *Computer-Controlled Systems: Theory and Design*. Prentice Hall, 2nd edition, 1990.

